Regime Change of the Boreal Summer Hadley Circulation and Its Connection with the Tropical SST

RAN FENG

State Key Laboratory of Numerical Modeling for Atmospheric Sciences and Geophysical Fluid Dynamics, Institute of Atmospheric Physics, Chinese Academy of Sciences, and Graduate University of Chinese Academy of Sciences, Beijing, China

JIANPING LI

State Key Laboratory of Numerical Modeling for Atmospheric Sciences and Geophysical Fluid Dynamics, Institute of Atmospheric Physics, Chinese Academy of Sciences, Beijing, China

JINCHENG WANG

State Key Laboratory of Numerical Modeling for Atmospheric Sciences and Geophysical Fluid Dynamics, Institute of Atmospheric Physics, Chinese Academy of Sciences, and National Meteorological Centre, China Meteorological Administration, Beijing, China

(Manuscript received 30 July 2010, in final form 19 January 2011)

ABSTRACT

The year-to-year variability of the boreal summer [June–August (JJA)] Hadley circulation (HC) is dominated by an asymmetric mode centered in the Northern Hemisphere (AMN) and a quasi-symmetric mode centered at 5°N (QSM). The regime change of the JJA HC is revealed by the phase reversal of the time series of the AMN, showing significant weakening of the northern part of the JJA HC and a reversed seesaw relationship of the zonal-mean updraft over 10°–20°N and around the equator. This transition is accompanied by the southward retreat of the HC core and is well correlated with the weakening of tropical summer monsoons. The strong warming trends of the sea surface temperature over the tropical Atlantic and Indo–west Pacific warm pool play an important role in the regime change of the JJA HC. The high-frequency interannual variability of the JJA HC, however, is mainly featured by the QSM and is highly correlated with the Niño-3.4 index, implying that ENSO's influence is mainly on the high-frequency interannual time scale.

1. Introduction

The interdecadal variability of the Hadley circulation (HC) has been discussed in many studies. For example, Chen et al. (2002) show that since 1985, there is an increasing trend of the outgoing longwave radiation and a decreasing trend of the reflected shortwave radiation within the tropics, suggesting an intensification of the tropical circulation. In particular, Quan et al. (2004) argue that the boreal winter [December–February (DJF)] HC has strengthened since the 1950s, inferred from the National Centers for Environmental Prediction–National Center for Atmospheric Research (NCEP–NCAR) Global Reanalysis 1 (NCEP-1) data. The strengthening of the DJF HC over different subperiods within the period of 1948–2003 for both NCEP-1 and the 40-yr European Centre for Medium-Range Weather Forecasts (ECWMF) Re-Analysis (ERA-40) data is further reported by Mitas and Clement (2005).

Different from the DJF HC, the intensity of boreal summer [June–August (JJA)] HC only shows minor changes (Quan et al. 2004; Mitas and Clement 2005, 2006; Tanaka et al. 2004). However, by using divergent wind shears as indices, Zhao and Moore (2008) find evident weakening trends of the regional meridional circulations over 90°–150°E, 15°W–40°E, and 120°–40°W from NCEP-1. These trends are consistent with precipitation records of corresponding regions from the Global

Corresponding author address: Dr. Jianping Li, State Key Laboratory of Numerical Modeling for Atmospheric Sciences and Geophysical Fluid Dynamics, Institute of Atmospheric Physics, Chinese Academy of Sciences, Beijing, China.
E-mail: ljp@lasg.iap.ac.cn

DOI: 10.1175/2011JCLI3959.1

Precipitation Climatology Project. The widespread weakening trends of the regional meridional circulation are indicative of a possible decadal variation of the JJA HC other than overall intensity; therefore, the empirical orthogonal function (EOF) is used in this study to recognize patterns of the JJA HC variations.

By EOF analysis of the monthly climatology of the mass streamfunction (MSF), Dima and Wallace (2003) show that the annual march of HC is dominated by two components of comparable mean-square amplitudes: one is equatorial symmetric with little seasonal variation and another is equatorial asymmetric, sinusoidally varying with seasons. Ma and Li (2007, 2008) report that the principal modes of the year-to-year variability of the DJF HC also contain an equatorial asymmetric mode and a symmetric mode, representing the decadal variability and the high-frequency interannual variability, respectively. The principal modes of variability of the JJA HC, however, have not yet been reported.

Before investigating the principal modes of variability of the JJA HC, caution should be used with regard to the reliability of NCEP-1 and ERA-40 in describing the decadal variability of the HC. The strengthening of the HC derived from these two reanalyses can be artificial. Held and Soden (2006) studied the responses of the hydrological cycle to the global warming condition, concluding that the decreasing in convective mass fluxes indicates the weakening rather than the strengthening of tropical circulation. Mitas and Clement (2006) report fundamental differences between most models of the Program for Climate Model Diagnosis and Intercomparison (PCMDI) and both the NCEP-1 and ERA-40 in describing the thermodynamic structure of the DJF tropical atmosphere. In their study, the instrumental systematic biases of the radiosonde observation data (Santer et al. 2005) damp the temperature trends at middle to high levels of the tropical troposphere in both reanalyses; as a result, the unstable tropical lapse rate inappropriately nudges the model toward the artificial strengthening of the DJF HC. A similar mechanism is also indicated by Held and Soden (2006).

However, the JJA HC does not show a significant strengthening trend (Quan et al. 2004; Mitas and Clement 2005, 2006; Tanaka et al. 2004), especially for NCEP-1. The intensity of the JJA HC shows a minor change (0.42% each year) within the simulated range of −4.83%–0.48% each year from 13 models of the Atmospheric Model Intercomparison Project (AMIP; Gates et al. 1999) for the period of 1979–98 (Table 1), which indicates that the upper-level data biases associated with the artificial strengthening of the HC are not a serious problem for the JJA HC compared with the DJF HC. However, ERA-40 shows a much stronger strengthening of 2.24% per year for the same period. Because particular caution should be paid to the artificial intensification of the HC calculated from the reanalysis, ERA-40 is not used in this study.

TABLE 1. Correlations of patterns (AMN and QSM) and time series (AMNI and QSMI) of the principal modes of the JJA HC between AMIP model results and NCEP-1 for the period of 1979–98. Here R = correlation of patterns; r = correlation of time series. Models not previously defined: Centre National de Recherches Météorologiques Coupled Global Climate Model, version 3 (CNRM-CM3); Institute of Numerical Mathematics Coupled Model, version 3 (INM-CM3); Model for Interdisciplinary Research on Climate 3.0, high-resolution version [MIROC3 (hires)]; Model for Interdisciplinary Research on Climate 3.0, medium-resolution version [MIROC3 (medres)]; Meteorological Research Institute Coupled General Circulation Model, version 2.0 (MRI CGCM2); Max Planck Institute ECHAM5 (MPI-ECHAM5); and NCAR Parallel Climate Model, version 1 (NCAR PCM1).

AMIP model	R_{AMN}	r_{AMNI}	R_{QSM}	r_{QSMI}
CNRM-CM3	0.81*	0.01	0.54*	0.05
GFDL CM2.1	0.93*	0.70*	0.86*	0.80*
GISS-ER	0.92*	0.64*	0.72*	0.57*
IAP FGOALS-g1.0	0.65*	0.53*	0.57*	0.47*
INM-CM3	0.92*	0.36	0.85*	0.45*
IPSL CM4	0.81*	0.71*	0.73*	0.65*
MIROC3 (hires)	0.84*	0.50*	0.55*	0.22
MIROC3 (medres)	0.88*	0.53*	0.05	0.50*
MRI CGCM2	0.88*	0.44	0.68*	0.32
MPI-ECHAM5	0.79*	0.29	0.59*	0.45*
NCAR CCSM3	0.14	0.26	0.80*	0.50*
NCAR PCM1	0.18	0.12	0.38	0.35
HadCM3	0.87*	0.71*	0.67*	0.53*

* Significant correlation above the 0.05 level.

In theoretic and simulation studies, patterns and amplitudes of sea surface temperature (SST) are shown to be closely connected with the intensity (e.g., Lindzen and Nigam 1987; Numaguti 1995), seasonality (Hou and Lindzen 1992; Numaguti 1995), and spatial structure of the HC (Broccoli et al. 2006; Lu et al. 2008; Mantsis and Clement 2009). In observations, variations of the tropical SST over the Indian Ocean significantly influence the intensity (Quan et al. 2004) and principal modes (Ma and Li 2008) of the DJF HC on a decadal time scale, whereas the SST over the tropical east Pacific (signal of ENSO) is closely associated with the interannual (Oort and Yienger 1996; Mitas and Clement 2005; Ma and Li 2008) and, presumably, decadal (Quan et al. 2004) variability of the HC; disagreement still exists on the latter viewpoint (Mitas and Clement 2005; Ma and Li 2008; Lu et al. 2008). Based on the principal modes of the JJA HC, the connection between the variability of the tropical SST and JJA HC is discussed in this paper. To distinguish direct contributions of the SST from contributions from

other factors, especially the radiative forcing, which is shown to be important to the expansion of the tropical band under the global warming condition (Lu et al. 2009), the results derived from the AMIP simulations are compared with those from the reanalysis.

For many studies, the NCEP-1 is not good enough to study the trend, which includes the intensity of the DJF HC, problems related to changes of equatorial Pacific surface wind (Wu and Xie 2003), and so on. However, we will show that the patterns and evolutions of the principal modes of the JJA HC are highly consistent across different datasets for the overlapped period, indicating that for our study, the dynamics represented by NCEP-1 can be reliable. Furthermore, the decadal variability of the JJA HC can be well explained by similar variations of the SST averaged over a wide range of tropical Indo–west Pacific warm pool and tropical Atlantic, which cannot merely be attributed to the data biases of NCEP-1.

This paper studies the principal modes and decadal variability of the JJA HC as well as their connections with the tropical SST. Section 2 describes the data and methods employed. Section 3 displays the principal modes of the JJA HC, and section 4 shows the decadal variability of the JJA HC. Contributions from the tropical SST to the principal modes of variability of the JJA HC are investigated in section 5, while section 6 provides conclusions and a discussion.

2. Data and methodology

a. Observational and model datasets

Three independent datasets are applied to analyze the principal modes of variability of the JJA HC: NCEP-1 (Kalnay et al. 1996) and the National Centers for Environmental Prediction–Department of Energy Global Reanalysis 2 (NCEP-2) (Kanamitsu et al. 2002) on a $2.5° \times 2.5°$ latitude–longitude grid with 17 vertical levels (www.cpc.ncep.noaa.gov/products/wesley/reanalysis2/kana/reanl2-1.htm), and the Japanese 25-yr Reanalysis (JRA-25; Onogi et al. 2007) on a $2.5° \times 2.5°$ latitude–longitude grid with 23 vertical levels. The principal modes and interdecadal variability of the JJA HC are analyzed based on NCEP-1 and verified by both NCEP-2 and JRA-25 for the overlapped period.

The SST data are extracted from the Met Office Hadley Center Sea Ice and SST dataset, version 1 (Rayner et al. 2003), which is on a $1.0° \times 1.0°$ latitude–longitude grid, to study the connections between the SST and variability of the JJA HC. We use model data of AMIP simulations for the Fourth Assessment Report (AR4) of the Intergovernmental Panel on Climate Change (IPCC) to distinguish the direct contribution of the SST from the radiative forcing to the principal modes of variability of the JJA HC. The AMIP is directed by the Working Group on Numerical Experimentation on behalf of the World Climate Research Programme (WCRP) to simulate the global climate using common boundary conditions and radiative forcing. The solar constant and atmospheric carbon dioxide concentration are fixed, while the real-time SST is applied as the boundary forcing. These experiments ensure the realistic oceanic forcing upon the circulation under the fixed direct effects of the atmospheric radiative forcing, and hence they can be a useful tool for our discussion on the influence of the SST on the variability of the JJA HC. The AMIP simulations of 13 models are analyzed here (Table 1); for models with multiple runs, atmospheric fields are averaged over all runs.

The Niño-3.4 index is used to indicate the ENSO phenomenon. This index is defined as SST anomalies over the Niño-3.4 region (5°S–5°N, 120°–170°W) based on the 1971–2000 base period (Enfield et al. 2001) (www.cpc.noaa.gov/data/indices/). The summer monsoon indices are defined as the area-averaged JJA dynamical normalized seasonality at 850 hPa (Li and Zeng 2000, 2002, 2003) over the South China Sea domain (0°–25°N, 100°–125°E), eastern part of the South Asia domain (2.5°–20°N, 70°–110°E), and the West Africa domain (5°–17.5°N, 20°W–40°E).

For the convenience of comparison, the period of extracting the principal modes of JJA HC from the reanalysis datasets and the AMIP simulations is 1979–98 [except for the atmospheric models of the Geophysical Fluid Dynamics Laboratory Climate Model, version 2.0 (GFDL CM2.0) (1980–98), and the NCAR Community Climate System Model, version 3 (CCSM3) (1979–97)]. Unless otherwise stated, the time evolution of the principal modes is calculated by projecting the anomalous MSF onto the principal modes of 1979–98. The SST and NCEP-1 data for the period of 1948–2007 are used to study the connection between the SST and variability of the principal modes of the JJA HC.

b. Methodology

Similar to previous studies (e.g., Peixoto and Oort 1992, 158–159; Li 2001), the mass streamfunction is calculated by a downward integration of the monthly meridional wind, using data at all available levels of analysis and simulations. The MSF are then averaged over JJA for each year. The EOF analysis is performed via the covariance matrix of the JJA mean MSF. The values at each grid point are weighted by the square root of the cosine of latitude. The MSFs of different models are bilinearly interpolated to the same height–latitude grid

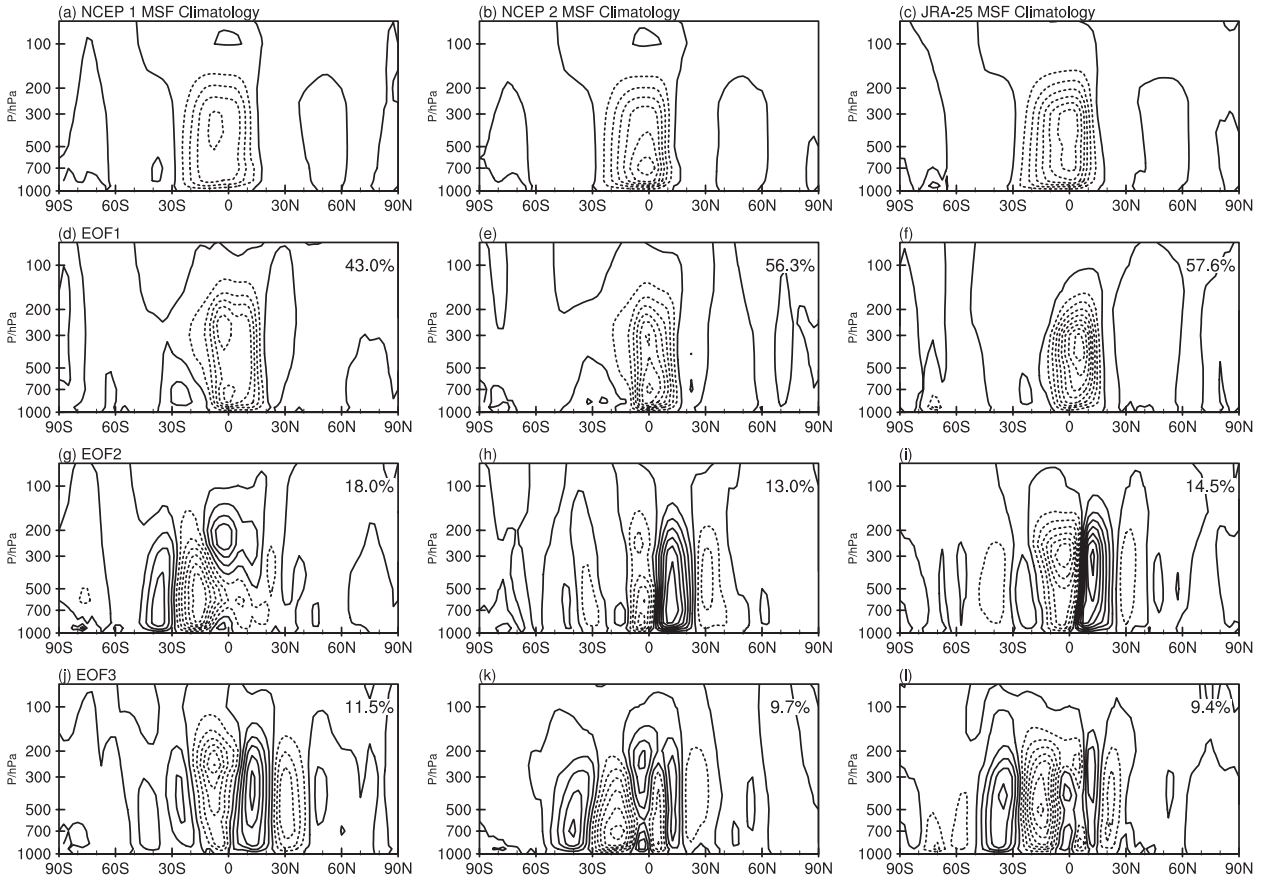

FIG. 1. JJA climatology of the MSF from (a) NCEP-1, (b) NCEP-2, and (c) JRA-25. The (d) first, (g) second, and (j) third EOF mode of the JJA MMC from NCEP-1. (e),(h),(k) As in (d),(g),(j), but for NCEP-2. (f),(i),(l) As in (d),(g),(i), but for JRA-25. Ratios of explained variance to the total are shown at the top-right corner of the picture of each EOF mode. Period is 1979–98 for all computations. Contour interval is 4×10^{10} kg s^{-1} in (a)–(c) and 0.025 kg s^{-1} in (d)–(l).

as NCEP-1 and then averaged to get the ensemble MSF. Via EOF analysis of the ensemble MSF, we get the principal modes of the simulated ensemble JJA HC. Correlation analysis is employed to investigate the relationship between the principal modes of the JJA HC and the SST. The correlation between two spatial fields of the HC modes is estimated by ranking all grid points of each field in the same order and computing the Pearson correlation coefficient between two series; as for our study, only grid points within 30°S–30°N are considered.

The index of the JJA HC intensity (HCI) is defined as the absolute value of the minimum of the JJA MSF between 30°S and the equator (Oort and Yienger 1996). The trends are computed using least squares linear regression. The statistical significance of values of the linear trend and correlation are assessed by means of a two-sided Student's *t* test, taking into account lag-1 (year) serial correlation (e.g., Bretherton et al. 1999). This procedure compensates for the temporal autocorrelation of many geophysical time series and reduces the degrees of freedom.

3. The principal modes of the year-to-year variability of the JJA HC

Figure 1 shows the climatological JJA MSF and the principal modes of the mean meridional circulation (MMC) computed using the NCEP-1, NCEP-2, and JRA-25 datasets for the period of 1979–98. Of all the datasets, the southern branch of the HC dominates the meridional circulation, extending from 30°S to about 15°N, while the northern branch of the HC is very weak and narrow; thus, the following analysis will focus on the southern branch of the HC and use ''HC'' for short.

All three datasets show an asymmetric mode (EOF1) dominating the variability of the JJA HC. This mode extends from 10°S to 20°N with centers in the Northern Hemisphere. It is referred to as the asymmetric mode in the Northern Hemisphere (AMN) and its principal component (PC) is referred to as the AMN index (AMNI). The second mode of NCEP-2 and JRA-25 is a quasi-symmetric mode with its axis slightly north of

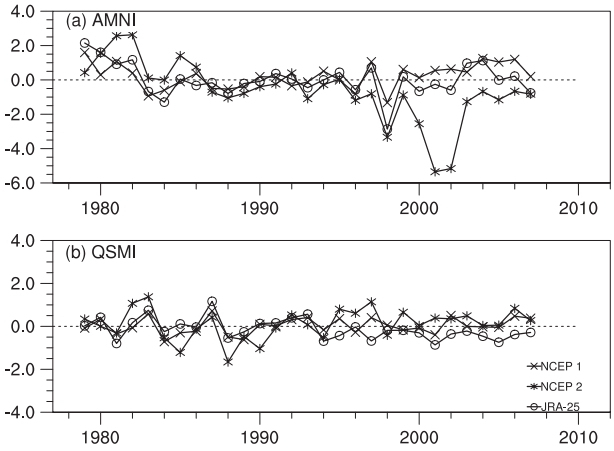

FIG. 2. (a) AMNI of the JJA HC from NCEP-1 (cross), NCEP-2 (asterisk), and JRA-25 (open circle) over the period of 1979–2007. (b) As in (a), but for QSMI.

the equator at about 5°N. It contains a pair of comparable circulations ranging from 15°S to 20°N and is referred to as the quasi-symmetric mode (QSM) and the PC is referred to as the QSM index (QSMI). North of the QSM, there are circulation anomalies of the Ferrel cell. The QSM appears in NCEP-1 data as the third mode with a similar spatial structure to the QSM of NCEP-2 and JRA-25, while the third mode of NCEP-2 and JRA-25 resembles the second mode of NCEP-1 in the Southern Hemisphere, with both a well-defined anomalous circulation ranging from 30° to 10°S and an anomalous Ferrel circulation south of it. However, north of 10°S, the spatial structures of this mode are quite different across the datasets, indicating that this mode is less identifiable from different datasets compared with the AMN and QSM; thus, the following analysis will focus on the AMN and QSM.

The time series of the AMNI (Fig. 2a) and QSMI (Fig. 2b) from NCEP-1, NCEP-2, and JRA-25 over the period of 1979–2007 are shown. The time evolutions of the AMNI and QSMI are similar across different reanalysis data for the overlapped period. All indicate a higher AMNI phase before the early 1980s, which can possibly be traced to the early years. As for the QSMI, there is no noticeable decadal signal but evident interannual variability. Similarities of the spatial structure and time evolution of the AMN and QSM across different datasets validate the existence of both modes. Since NCEP-1 spans a longer period, we mainly use it to study the decadal variability of the JJA HC.

To test the stabilities of the spatial structure of the AMN and QSM over time, the EOF analysis has been performed on the JJA MSF for the periods of 1948–2007, 1959–2007, 1970–2007 and 1979–2007 of NCEP-1.

TABLE 2. Correlations of patterns between the base AMN, QSM over the period of 1979–98 and AMN, QSM over periods of 1948–2007, 1959–2007, 1970–2007, and 1979–2007. All results are derived from NCEP-1; R = correlation of patterns.

	1948–2007	1959–2007	1970–2007	1979–2007
R_{AMN}	0.87	0.94	0.95	0.95
R_{QSM}	0.82	0.51	0.93	0.94

The patterns of AMN and QSM for the period of 1979–1998 are correlated with the corresponding AMN and QSM for other periods. High correlation coefficients (Table 2) suggest the considerable stability of the AMN and QSM. Since the AMN and QSM derived from 1979–1998 are directly comparable to the AMIP model results, we use them as the base modes. By projecting the JJA MSF anomalies (with respect to the mean MSF of 1948–2007) onto these two base modes, we get time series of the AMNI and QSMI for 1948–2007.

The AMN of the JJA HC can be further understood by the seesaw relationship of the vertical pressure velocity ω between 10° and 20°N and around the equator. Figure 3 shows cross correlations between the zonal averaged ω of the three independent datasets for the periods of 1948–2007, 1979–2007, and 1979–98 at various latitudes within the tropics. The outstanding feature is the significant negative correlations of the zonal-mean vertical motions between 10° and 20°N and 10°S and 10°N. In particular, there are two centers of negative correlations: one locates at 15°N and the other around the equator for all datasets and periods. In Figs. 1 and 3, the ω at 10°–20°N and 10°S–0° for the period of 1979–1998 corresponds to the anomalous updraft branch and the subsidence branch, respectively, of the positive phase of the AMN for the same period. The seesaw relationship of ω between 10° and 20°N and around the equator adds additional evidence to the existence of the AMN, given the MSF is computed from the meridional wind. Alternatively, the AMN reflects a salient seesaw relationship of the zonal-mean vertical motion: with the strengthening of the updraft over 10°–20°N, the updraft around the equator weakens and vice versa.

4. Regime change of the JJA HC

Figure 4 shows the time series of the reconstructed AMNI and QSMI from NCEP-1 data. Around 1970, an evident phase reversal of the AMNI can be clearly identified from NCEP-1, as the 9-yr filtered AMNI changed from above normal to below normal. Figure 4b shows the time series of the 500-hPa vertical pressure velocities averaged over 10°–20°N and 5°S–5°N. From 1948 to the end of the 1960s, with the positive phase of

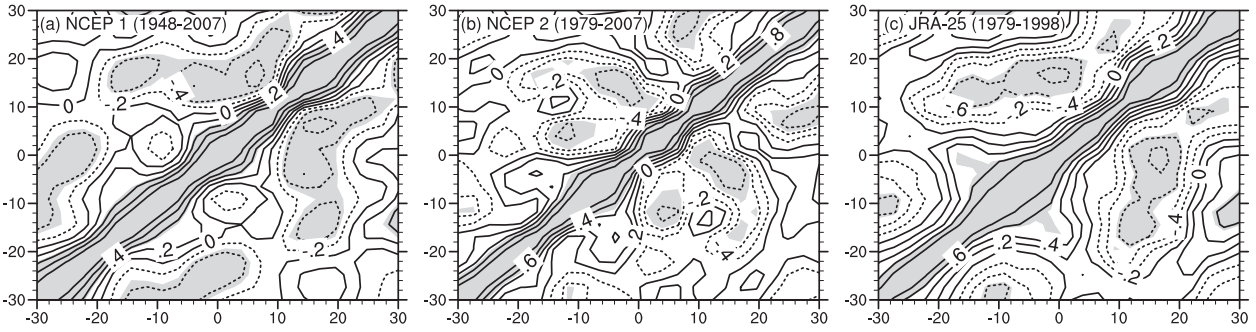

FIG. 3. (a) Correlations between the JJA zonal-mean vertical pressure velocities at all latitudes within the tropics (30°S–30°N) from NCEP-1 over the period of 1948–2007. (b),(c) As in (a) but for NCEP-2 (1979–2007) and JRA-25 (1979–98). Contour level is 0.2. Values above 98% confidence level are shaded.

the AMNI, an anomalous updraft over 10°–20°N (Fig. 4b) and subsidence over 5°S–5°N construct a strengthened HC northern part. However, from the 1970s to the early 1980s, the AMNI changed into a negative phase with an anomalous updraft over 5°S–5°N and subsidence over 10°–20°N. The shift of the AMNI in the early 1980s is also evident in NCEP-2 and JRA-25 (Fig. 2a); thus, it is less likely to be a result of systematic biases of the NCEP-1 data due to the assimilation of satellite data since 1979. The stepwise evolution of the intensity of the JJA HC in the 1970s, in the work by Quan et al.(2004), has been described as the ''regime change'' (similar to Fig. 4a); here we use this term to describe the changes of the spatial structures of the circulation cell from a strong northern part toward a weak northern part.

The regime change of the JJA HC can be further explained by the southward retreat of the HC core, which is defined by the mean latitude of all tropical grid points (30°S–30°N) with the absolute MSF value exceeding a certain percentage of the HCI. By using 90%, 80%, 70%, 60%, and 50% HCI as criteria, significant southward trends can be identified at or above the 95% confidence level (Fig. 4c). Accompanied with the southward retreat of the HC core, half of the mass transportation moves farther south, contributing to a weaker northern part.

To understand how much of the local circulation variability is a manifestation of the regime change of the JJA HC, correlations between the AMNI and tropical summer monsoons are investigated. Although the Asia summer monsoon, which covers both tropical and extratropical latitudes (10°–30°N, 70°–110°E), has long been considered as the counterpart of the northern branch of the HC (e.g., Goswami et al. 1999), the tropical monsoons shown by Dima and Wallace (2003) are closely connected with the cross-equatorial asymmetric mode of the southern branch of the HC. Here the AMNI is highly correlated with the South China Sea summer monsoon index (SCSSMI), the South Asian summer monsoon index 2 (SASMI2), and the West African summer monsoon index (WASMI) (Li and Zeng 2002, 2003, 2005) with coefficients of 0.43, 0.49 and 0.52, respectively. The trends for the SASMI2, SCSSMI, and WASMI are −0.21, −0.25, and −0.69, respectively, over the period of 1948–2007—all significant above the 99% confidence level. The WASMI changes to below normal in the late 1960s, while trends of the SASMI and SCSSMI drop to below normal in the 1970s (Fig. 5). Studies have revealed the widespread weakening trends of the Asian summer monsoon (Nitta and Hu 1996; Wang 2001) and Sahel rainfall

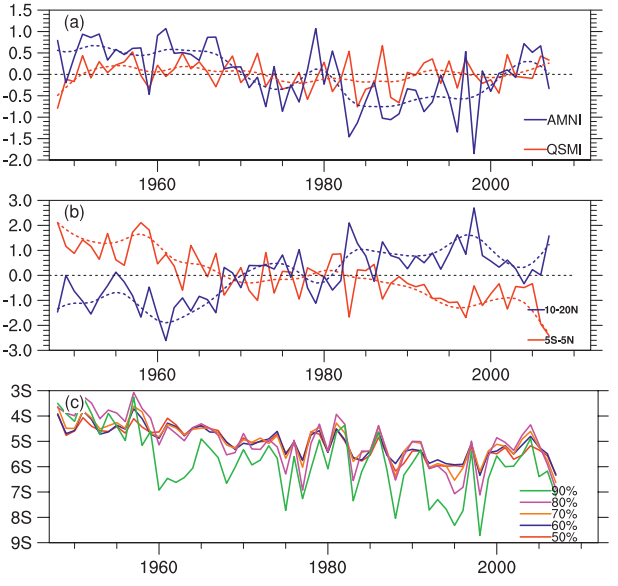

FIG. 4. (a) Time series of the JJA AMNI (blue) and QSMI (red) from NCEP-1 over 1948–2007. (b) Standardized JJA zonal-mean vertical pressure velocity at 500-hPa level averaged over 5°S–5°N (red) and 10°–20°N (blue) latitudes. (c) Time series of the core latitudes of 50%–90% zonal-mean mass transport by the JJA HC. Dashed lines in (a)–(c) are 9-yr Gaussian-filtered results for the time series in the same color.

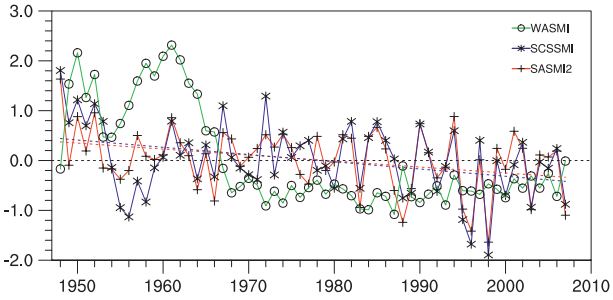

FIG. 5. Time series of the JJA SCSSMI (red), SASMI2 (blue) and WASMI (green). Trends of the SASMI2 (blue) and SCSSMI (red) are also shown.

(e.g., Lamb 1982; Nicholson et al. 2000) in the 1970s. The significant correlations and similar periods of the changing phase of the AMNI and three monsoon indices indicate that the observed decadal weakening of tropical monsoons may not happen independently but as manifestations of the variability of zonal-mean background circulation.

5. Connection with the tropical SST

Given that the SST pattern has significant influences on the dynamics (Lindzen and Nigam 1987; Hou and Lindzen 1992; Numaguti 1995) and simulated variability (Quan et al. 2004; Mantsis and Clement 2009) of the HC, we further focus on the connections between the AMN, the QSM, and the SST. To distinguish the direct contributions of the SST variability from others, especially the radiative forcing, we analyzed the simulated principal modes of the JJA HC using 13 models of the AMIP experiments. The limited time span of the AMIP experiments prohibits its application of validating the regime change of the JJA HC from the 1970s to the early 1980s; nevertheless, those experiments provide valuable insights into the connection between the SST forcing and the variation of the JJA HC.

Table 1 displays correlation coefficients of patterns and time series between the first (second) mode of the JJA HC computed using AMIP simulations and the AMN (QSM) as well as between the PC1 (PC2) and AMNI (QSMI). Most of the models can produce similar patterns of the AMN and QSM. Among them, the GFDL CM2.1, the Goddard Institute for Space Studies Model E-R (GISS-ER), the Institute of Atmospheric Physics Flexible Global Ocean–Atmosphere–Land System Model, gridpoint version 1.0 (IAP FGOALS-g1.0), the L'Institut Pierre-Simon Laplace Coupled Model, version 4 (IPSL CM4), as well as the third climate configuration of the Met Office Unified Model (HadCM3) show high correlations with both the patterns and time series of the AMN and QSM; thus, these model results are used to construct the ensemble mean MSF. The full model years of each member as well as the AMNI and QSMI calculated by individual models are displayed in Fig. 6; the ensemble mean MSF of 1979–2000 is computed by averaging the model results for the overlapped periods. By EOF analysis of the ensemble MSF, we get the ensemble AMN and QSM (Fig. 6) as well as AMNI and AMSI (Fig. 7). It is clear that the ensemble AMN and QSM highly resemble the AMN and QSM from reanalysis data for the same period. Correlations of the AMNI and QSMI between model ensemble results and NCEP-1 are as high as 0.67 and 0.68, respectively. Given that the SST-forced experiments reproduce the AMN, the QSM, and their variations in a way that is comparable to observations, it is possible that the SST plays a major role in driving the variability of the AMNI and QSMI.

To further investigate the region where SST is of particular importance to the variability of the AMN and QSM over time, the AMNI and QSMI are correlated with the JJA SST field over the period of 1948–2007 of NCEP-1 (Figs. 8a and 8b). Significant correlations between the AMNI and SST are found over the Indo–west Pacific warm pool, tropical Atlantic Ocean, and the southwest tropical Indian Ocean. The SST over all three regions has significant warming trends (Fig. 8c). With reference to Fig. 3, the SST variability over the equatorial Indo–west Pacific warm pool and the tropical

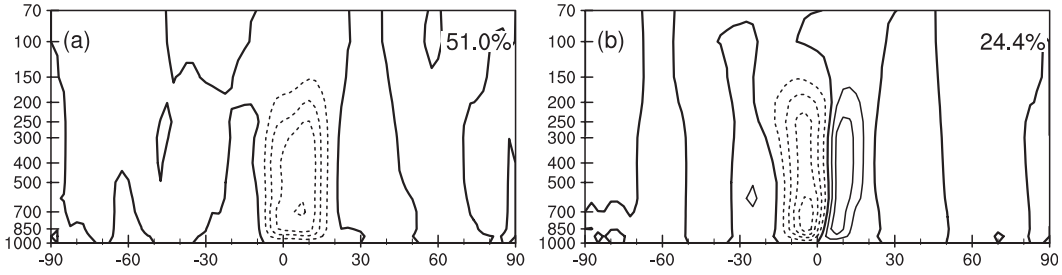

FIG. 6. (a) First and (b) second modes of the ensemble-averaged MSF for GFDL CM2.1, GISS-ER, IPSL CM4, IAP FGOALS-g1.0, and HadCM3 over 1979–2000. Ratio of the explained variation of each mode to the total is given at the top-right corner. Contour level is 0.04.

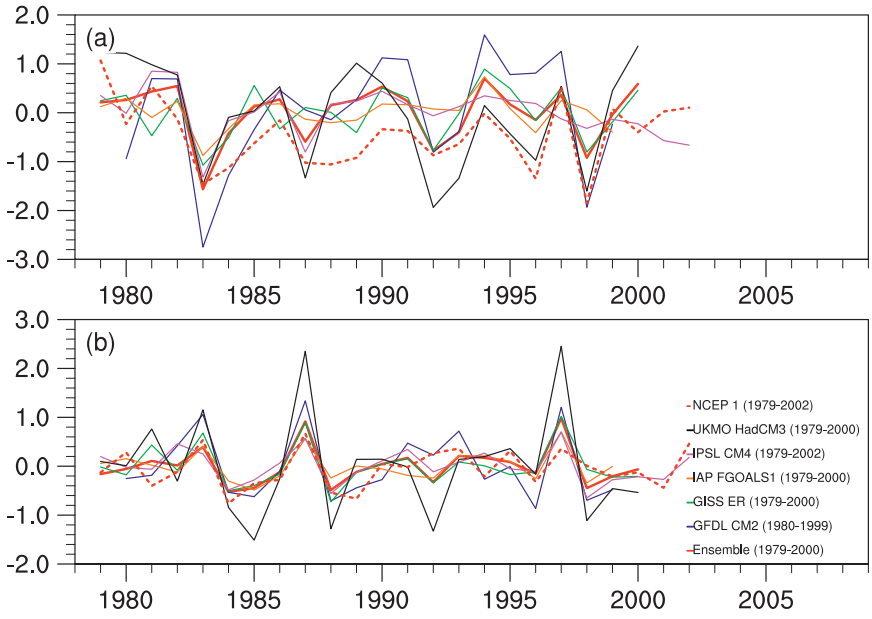

FIG. 7. Time series of the (a) JJA AMNI and (b) QSMI of each ensemble component, the ensemble mean MSF, and NCEP-1. Time span of each time series is indicated.

Atlantic can be very important given that it modulates vertical motions around the equator. Through the seesaw connection of the vertical motions around the equator and over 10°–20°N, the SST changes over the equatorial Indo–west Pacific warm pool and tropical Atlantic can also influence the vertical motions at 10°–20°N. The vertical motions of these two latitude bands then construct a stronger or weaker circulation anomaly represented by the AMN. The time series of the SST averaged over the Indo–west Pacific warm pool and tropical Atlantic (10°S–10°N, 40°W–160°E) is highly correlated with the reconstructed AMNI at a coefficient of 0.55 for 1948–2007 and with the ensemble AMNI at a coefficient of 0.40 for 1979–2000. Figure 8c displays the time series of the SST averaged over 10°S–10°N, 40°W–160°E along with the 9-yr Gaussian-filtered zonal-mean vertical pressure velocity averaged over 10°S–10°N. The regime changes of both time series is evident and simultaneous from the late 1960s to the early 1980s, indicating that the SST warming by phase over the Indo–west Pacific warm pool and tropical Atlantic can be the main contributor to the stepwise enhancement of the equatorial upward motion and evolution of the AMN.

Significant correlations between the SST and QSMI (Fig. 3c), however, mainly cover the tropical eastern-central Pacific (10°S–10°N, 150°–80°W) and show a shape reminiscent of the typical SST anomaly pattern during the mature phase of El Niño. In addition, as for the AMNI and QSMI, only the QSMI possesses a high correlation with the Niño-3.4 with a coefficient of 0.55. Given that the QSMI mainly features the high-frequency interannual variability of the JJA HC; similar to the DJF HC (Ma and Li 2008), the influence of the ENSO signal on the JJA HC is mainly at a high-frequency interannual time scale.

6. Conclusions and discussion

This study investigates the year-to-year variability of the JJA HC. The results can be summarized as follows: the variability of the JJA HC is dominated by two principal modes. One of them is equatorial asymmetric centered in the Northern Hemisphere (AMN) and another is quasi-symmetric about the equator (QSM). The AMN reflects the seesaw relationship of the zonal-mean vertical motions between 10° and 20°N and around the equator. The regime change of the JJA HC from a stronger northern part to a weaker northern part is revealed by the trends of the zonal-mean vertical motions and the phase reversal of the AMN. The weakening of the tropical summer monsoons over the South China Sea, the eastern part of South Asia, and West Africa can be largely explained by this transition.

The sea surface temperature (SST) of the tropical Indo–west Pacific warm pool and tropical Atlantic (10°S–10°N, 40°W–160°E) is of particular importance to drive the variability of the AMN through the seesaw relationship of the vertical motions between 10° and 20°N and around the equator. The stepwise SST warming over this region enhances the equatorial updraft, while it reduces the updraft over 10°–20°N, which significantly contributes

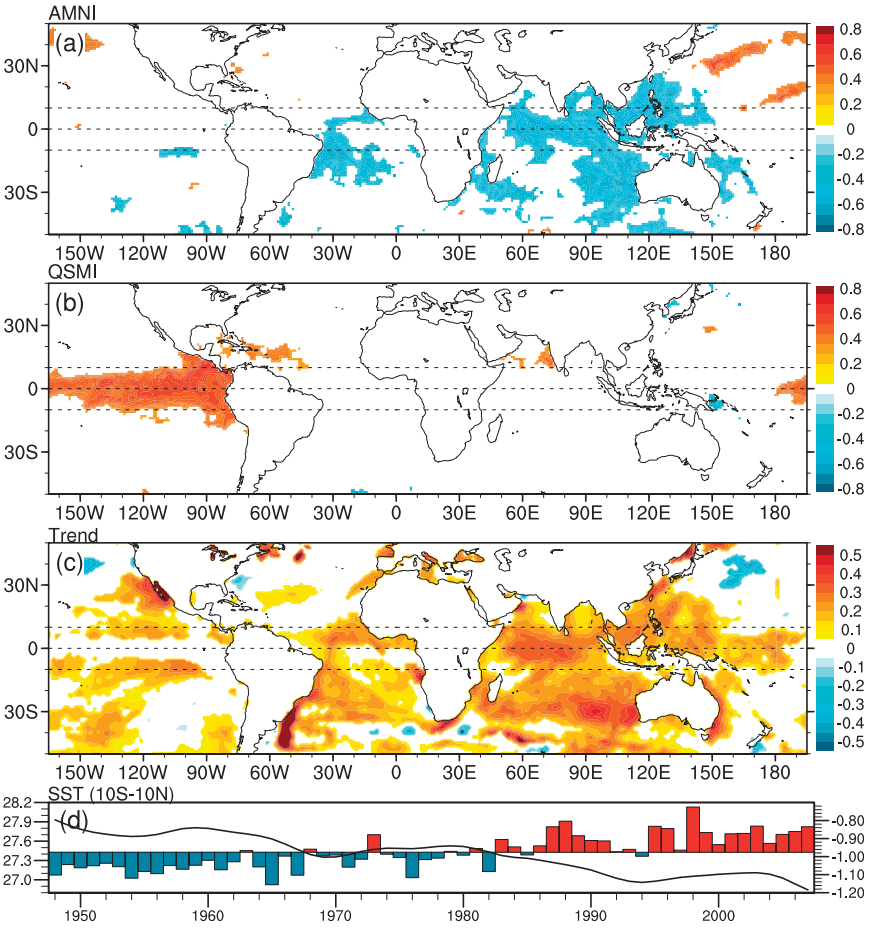

FIG. 8. Correlation maps between the JJA SST and the (a) AMNI and (b) QSMI. (c) Linear trends of the SST (0.01°C yr^{-1}). Values above the 95% confidence level in (a)–(c) are shaded. (d) Time series of the SST averaged over the equatorial Indo–west Pacific warm pool and tropical Atlantic (10°S–10°N, 40°W–160°E), and the 9-yr Gaussian-filtered zonal-mean 500-hPa vertical pressure velocity averaged over 10°S–10°N.

to a negative AMN phase. The QSM, however, mainly features the high-frequency interannual variability of the JJA HC and is highly correlated with the ENSO signal. This result indicates that the ENSO influence is mainly at a high-frequency interannual time scale.

In the work by Dima and Wallace (2003), although the solstical mode is also asymmetric about the equator, it spans much wider from about 25°S to 30°N and mainly reflects the seasonal reversal of the HC. When the year-to-year variability of the seasonal mean HC is considered, a seasonal reversal signal should not exist. Thus, the resulted asymmetric modes of DJF (Ma and Li 2008) and JJA HCs, in physics, are different from the asymmetric mode of the monthly HC climatology derived by Dima and Wallace (2003). Note that the AMN and asymmetric mode of the DJF HC spans about the same range, from 10°S to 20°N (Fig. 1 in Ma and Li 2008). And the seesaw relationship of the zonal-mean vertical motions between 10° and 20°N and around the equator during DJF is still evident (Fig. 9). Because both the AMN and asymmetric mode of the DJF HC contain the decadal variability of the HC, future studies on their dynamics can be important to understand the long-term behavior of the HC.

Previous studies (Knutson and Manabe 1998; Held and Soden 2006; Mitas and Clement 2005, 2006) suggest the weakening of the HC under the global warming condition. In the work by Held and Soden (2006), the warming of the temperature and the increasing of the lower-level moisture are associated with the reduction of the convective mass and the tropical circulations. However, Held and Soden (2006) and many of the other above-mentioned authors focus on the general tropical circulation, especially its intensity. Our work, rather than discussing the overall intensity, focuses on the spatial structure of the variations of the JJA HC. Held and Soden (2006), after

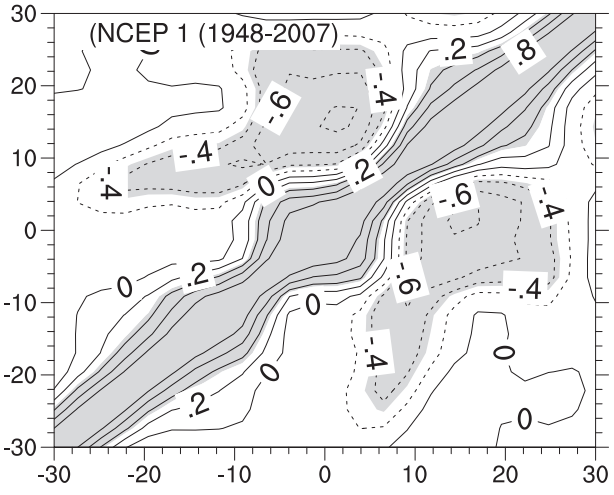

FIG. 9. Correlations between the DJF zonal-mean vertical pressure velocities at all latitudes within the tropics for NCEP-1 over the period of 1948–2007.

computing the spatial variance of the convective mass flux over the tropics, have recognized the redistribution of convection under the global warming condition. Although we are not sure to what extent the AMN can represent this scenario, we give a possible mechanism toward the redistribution of the tropical convection.

The importance of the tropical SST forcing on changing the AMN phase is emphasized here; however, we do not rule out contributions from the extratropical forcing, especially the Pacific decadal oscillation (PDO) (e.g., Hare and Mantua 2000), which shows the phase reversal as being roughly simultaneous with the AMN. The correlation coefficient between the AMNI and PDO index (http://jisao.washington.edu/pdo/) is −0.32. Although not high, the composite differences of the MSF between the high and low phases of the PDO (figure not shown) show similar patterns to the AMN. In this sense, the PDO may still contribute to the decadal variability of the JJA HC. In addition, the atmospheric stability over the extratropics is shown to be important to the width of the HC (Lu et al. 2007, 2008)—whether it influences the regime change of the JJA HC and whether detailed dynamical processes such as eddy momentum and heat transport (Schneider 2006) also contribute to this is open to further investigation.

Acknowledgments. We thank the editor and two anonymous referees, whose comments greatly improved the paper. This work was jointly supported by the 973 Program (Grant 2010CB950400) and the NSFC Projects (Grants 41030961 and 40821092).

REFERENCES

Bretherton, C. S., M. Widmann, V. P. Dymnikov, J. M. Wallace, and I. Bladé, 1999: The effective number of spatial degrees of freedom of a time-varying field. *J. Climate,* **12,** 1990–2009.

Broccoli, A. J., K. A. Dahl, and R. J. Stouffer, 2006: Response of the ITCZ to Northern Hemisphere cooling. *Geophys. Res. Lett.,* **33,** L01702, doi:10.1029/2005GL024546.

Chen, J. Y., B. E. Carlson, and A. D. Del Genio, 2002: Evidence for strengthening of the tropical general circulation in the 1990s. *Science,* **295,** 838–841.

Dima, I. M., and J. M. Wallace, 2003: On the seasonality of the Hadley cell. *J. Atmos. Sci.,* **60,** 1522–1527.

Enfield, D. B., A. M. Mestas-Nuñez, and P. J. Trimble, 2001: The Atlantic multidecadal oscillation and its relationship to rainfall and river flows in the continental U.S. *Geophys. Res. Lett.,* **28,** 2077–2080.

Gates, W. L., and Coauthors, 1999: An overview of the results of the Atmospheric Model Intercomparison Project (AMIP I). *Bull. Amer. Meteor. Soc.,* **80,** 29–55.

Goswami, B. N., V. Krishnamurthy, and H. Annmalai, 1999: A broad-scale circulation index for the interannual variability of the Indian summer monsoon. *Quart. J. Roy. Meteor. Soc.,* **125,** 611–633.

Hare, S. R., and N. J. Mantua, 2000: Empirical evidence for North Pacific regime shifts in 1977 and 1989. *Prog. Oceanogr.,* **47,** 103–145.

Held, I. M., and B. J. Soden, 2006: Robust responses of the hydrological cycle to global warming. *J. Climate,* **19,** 5686–5699.

Hou, A. Y., and R. S. Lindzen, 1992: The influence of concentrated heating on the Hadley circulation. *J. Atmos. Sci.,* **49,** 1233–1241.

Kalnay, E., and Coauthors, 1996: The NCEP/NCAR 40-Year Reanalysis Project. *Bull. Amer. Meteor. Soc.,* **77,** 437–472.

Kanamitsu, M., W. Ebisuzaki, J. Woollen, S.-K. Yang, J. J. Hnilo, M. Fiorino, and G. L. Potter, 2002: NCEP–DOE AMIP-II Reanalysis (R-2). *Bull. Amer. Meteor. Soc.,* **83,** 1631–1643.

Knutson, T. R., and S. Manabe, 1998: Model assessment of decadal variability and trends in the tropical Pacific Ocean. *J. Climate,* **11,** 2273–2296.

Lamb, P. J., 1982: Persistence of Subsaharan drought. *Nature,* **299,** 46–48.

Li, J., 2001: *Atlas of Climate of Global Atmospheric Circulation I* (in Chinese). China Meteorology Press, 279 pp.

——, and Q. Zeng, 2000: Significance of the normalized seasonality of wind field and its rationality for characterizing the monsoon. *Sci. China,* **43D,** 646–653.

——, and ——, 2002: A unified monsoon index. *Geophys. Res. Lett.,* **29,** 1274, doi:10.1029/2001GL013874.

——, and ——, 2003: A new monsoon index and the geographical distribution of the global monsoons. *Adv. Atmos. Sci.,* **20,** 299–302.

——, and ——, 2005: A new monsoon index, its interannual variability and relation with monsoon precipitation. *Climatic Environ. Res.,* **10,** 351–365.

Lindzen, R. S., and S. Nigam, 1987: On the role of sea surface temperature gradients in forcing low-level winds and convergence in the tropics. *J. Atmos. Sci.,* **44,** 2418–2436.

Lu, J., G. A. Vecchi, and T. Reichler, 2007: Expansion of the Hadley cell under global warming. *Geophys. Res. Lett.,* **34,** L06805, doi:10.1029/2006GL028443.

——, G. Chen, and D. M. W. Frierson, 2008: Response of the zonal mean atmospheric circulation to El Niño versus global warming. *J. Climate,* **21,** 5835–5851.

——, C. Deser, and T. Reichler, 2009: Cause of the widening of the tropical belt since 1958. *Geophys. Res. Lett.,* **36,** L03803, doi:10.1029/2008GL036076.

Ma, J., and J. Li, 2007: Strengthening of the boreal winter Hadley circulation and its connection with ENSO. *Prog. Nat. Sci.,* **17,** 1327–1333.

——, and ——, 2008: The principal modes of variability of the boreal winter Hadley cell. *Geophys. Res. Lett.,* **35,** L01808, doi:10.1029/2007GL031883.

Mantsis, D. F., and A. C. Clement, 2009: Simulated variability in the mean atmospheric meridional circulation over the 20th century. *Geophys. Res. Lett.,* **36,** L06704, doi:10.1029/2008GL036741.

Mitas, C. M., and A. Clement, 2005: Has the Hadley cell been strengthening in recent decades? *Geophys. Res. Lett.,* **32,** L03809, doi:10.1029/2004GL021765.

——, and ——, 2006: Recent behavior of the Hadley cell and tropical thermodynamics in climate models and reanalyses. *Geophys. Res. Lett.,* **33,** L01810, doi:10.1029/2005GL024406.

Nicholson, S. E., B. Somé, and B. Kone, 2000: An analysis of recent rainfall conditions in West Africa, including the rainy seasons of the 1997 El Niño and the 1998 La Niña years. *J. Climate,* **13,** 2628–2640.

Nitta, T., and Z.-Z. Hu, 1996: Summer climate variability in China and its association with 500 hPa height and tropical convection. *J. Meteor. Soc. Japan,* **74,** 425–445.

Numaguti, A., 1995: Dynamics and energy balance of the Hadley circulation and the tropical precipitation zones. Part II: Sensitivity to meridional SST distribution. *J. Atmos. Sci.,* **52,** 1128–1141.

Onogi, K., and Coauthors, 2007: The JRA-25 Reanalysis. *J. Meteor. Soc. Japan,* **85,** 369–432.

Oort, A. H., and J. J. Yienger, 1996: Observed interannual variability in the Hadley circulation and its connection to ENSO. *J. Climate,* **9,** 2751–2767.

Peixoto, J. P., and A. H. Oort, 1992: *Physics of Climate*. American Institute of Physics, 520 pp.

Quan, X.-W., H. F. Diaz, and M. P. Hoerling, 2004: Change in the tropical Hadley cell since 1950. *The Hadley Circulation: Past, Present, and Future,* H. F. Diaz and R. S. Bradley, Eds., Cambridge University Press, 85–120.

Rayner, N. A., D. E. Parker, E. B. Horton, C. K. Folland, L. V. Alexander, D. P. Rowell, E. C. Kent, and A. Kaplan, 2003: Global analyses of sea surface temperature, sea ice, and night marine air temperature since the late nineteenth century. *J. Geophys. Res.,* **108,** 4407, doi:10.1029/2002JD002670.

Santer, B. D., and Coauthors, 2005: Amplification of surface temperature trends and variability in the tropical atmosphere. *Science,* **309,** 1551–1556.

Schneider, T., 2006: The general circulation of the atmosphere. *Annu. Rev. Earth Planet. Sci.,* **34,** 655–688.

Tanaka, H. L., N. Ishizaki, and A. Kitoh, 2004: Trend and interannual variability of Walker, monsoon and Hadley circulations defined by velocity potential in the upper troposphere. *Tellus,* **56A,** 250–269.

Wang, H. J., 2001: The weakening of the Asian monsoon circulation after the end of 1970's. *Adv. Atmos. Sci.,* **18,** 376–386.

Wu, R., and S.-P. Xie, 2003: On equatorial Pacific surface wind changes around 1977: NCEP–NCAR reanalysis versus COADS observations. *J. Climate,* **16,** 167–173.

Zhao, H. X., and G. W. K. Moore, 2008: Trends in the boreal summer regional Hadley and Walker circulations as expressed in precipitation records from Asia and Africa during the latter half of the 20th century. *Int. J. Climatol.,* **28,** 563–578.